

## **In situ investigation of the discharge of alkaline Zn–MnO<sub>2</sub> batteries with synchrotron x-ray and neutron tomographies**

I. Manke<sup>a)</sup> and J. Banhart

*Institute of Materials Science and Technology, Technical University Berlin, 10623 Berlin, Germany*

A. Haibel, A. Rack,<sup>b)</sup> S. Zabler, N. Kardjilov, and A. Hilger

*Hahn-Meitner-Institut, 14109 Berlin, Germany*

A. Melzer

*Grillo-Werke AG, 38644 Goslar, Germany*

H. Riesemeier

*Federal Institute for Materials Research and Testing, 12205 Berlin, Germany*

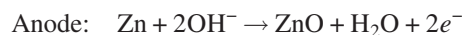
(Received 22 December 2006; accepted 27 April 2007; published online 21 May 2007)

Zn–MnO<sub>2</sub> alkaline batteries were investigated *in situ* at different stages of electric discharge by synchrotron tomography with monochromatic x rays and by neutron tomography. The spatial distribution and the changes in the morphology of different components of a battery caused by the reduction of MnO<sub>2</sub>, the dissolution of Zn, and the nucleation and growth of ZnO are investigated with high spatial resolution around several micrometers with x rays. Neutron tomography is used to monitor the changes in the spatial distribution of hydrogen in the MnO<sub>2</sub> matrix and provides complementary information about the process. © 2007 American Institute of Physics.

[DOI: 10.1063/1.2742283]

Alkaline Zn–MnO<sub>2</sub> batteries are still one of the most used battery types. Many advances have been made to enhance the lifetime especially under high power and high drain rates.<sup>1–4</sup> Progress in the development of rechargeable alkaline batteries offers interesting possibilities for future applications<sup>1,5</sup> which is the reason for the extent of current work focused on both rechargeable and not rechargeable alkaline battery types.<sup>1–13</sup>

Alkaline batteries consist of MnO<sub>2</sub> at the cathode and Zn powder at the anode.<sup>14,15</sup> While MnO<sub>2</sub> is used as a solid mixture with graphite; the Zn powder is suspended in gelled KOH electrolyte. During electric discharge MnO<sub>2</sub> is reduced by a solid-state intercalation of H<sup>+</sup> into the MnO<sub>2</sub> lattice, while at the anode zinc is oxidized by a dissolution-precipitation process. The main chemical processes are described by



Further details on the complex chemical processes are given in the literature.<sup>5,14</sup>

Investigations of the oxidation of the zinc, reduction of the MnO<sub>2</sub>, and the influence of different chemical additives on both are current research topics.<sup>1–3,5,7–11</sup> The knowledge about morphology and spatial distribution of the different chemical components is of great importance.<sup>1,9</sup>

Electron microscopy and optical microscopy are widely used to characterize the nucleation and growth process of ZnO.<sup>1,16,17</sup> The drawback of these techniques is that they do not allow for an *in situ* study of the material inside the entire volume of the battery. Once the sample has been cut it cannot

be used for the investigation of further discharge stages. Furthermore sample preparation is difficult because the surface is unstable in air. Oxidation and corrosion of Zn and carbonation of ZnO change the chemical compositions of the materials at the surface. In addition, the electrolyte KOH has to be removed without changing the chemical components. An *ex situ* method to overcome some of these problems was developed recently by Horn and Shao-Horn.<sup>1</sup>

*In situ* Raman spectroscopy, *in situ* X-ray absorption spectroscopy, and *in situ* synchrotron x-ray diffraction have been used for investigations of both alkaline and Li batteries by several groups.<sup>2,7,10,18</sup> Laboratory x-ray microtomography and two-dimensional neutron radiography<sup>19–21</sup> provided additional insights but with the limit of low resolutions around 100–200 μm. However, Sinha *et al.* used x-ray microtomography with rather high spatial resolution of around 10 μm for investigation of fuel cell materials.<sup>22</sup>

In this letter we apply synchrotron x-ray tomography for *in situ* investigations of the three-dimensional spatial distribution of different chemical components inside an alkaline battery.<sup>23</sup> The high spatial resolution in combination with the high density contrast due to the use of monochromatic x rays allows us to give an analysis of the changes of morphology and chemistry inside the battery. Because this method is non-destructive the batteries can be investigated during discharge. In contrast to x rays neutrons are strongly attenuated by hydrogen. Therefore, neutron tomography was used to investigate also *in situ* the hydrogen transport from the anode to the cathode and the distribution of the intercalated hydrogen in the MnO<sub>2</sub> matrix, thus providing information complementary to synchrotron x-ray tomography.

Synchrotron x-ray tomography was performed at the “BAMline” at the electron storage ring BESSY (Berlin, Germany) at an x-ray energy of 60 keV.<sup>24</sup> A Princeton Instruments charge coupled device (CCD) camera setup (2048 × 2048 pixels) with low magnifying optics and a BGO scin-

<sup>a)</sup>Electronic mail: manke@hmi.com

<sup>b)</sup>Present address: Forschungszentrum Karlsruhe, D-76344 Eggenstein-Leopoldshafen, Germany.

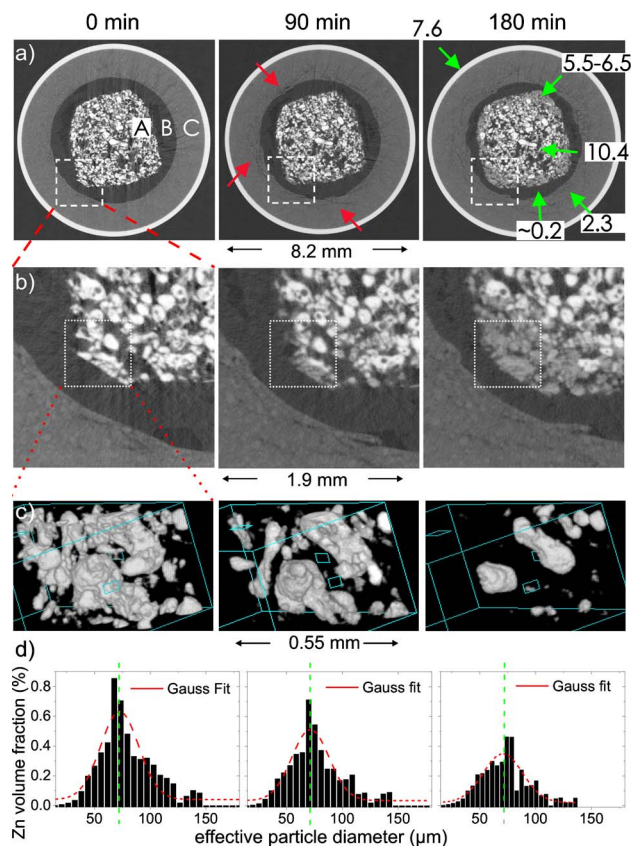


FIG. 1. (Color online) Zinc particles in an AAAA alkaline battery as imaged by synchrotron x-ray tomography. Completely charged battery and the same battery after two discharging steps (90 and 180 min) is shown: (a) Cross sections through the battery at the same position and measured attenuation coefficients for the different materials (in  $\text{cm}^{-1}$ ); (b) enlargements of the positions marked in (a); (c) 3D view of the zinc particles marked in (b); and (d) corresponding size distributions of the zinc particles for the three stages of discharge. Vertical dashed line represents the average diameters (first moment of the distribution).

tillator ( $\text{Bi}_4\text{Ge}_3\text{O}_{12}$ , thickness of  $100 \mu\text{m}$ ) were used in order to adapt the field of view to the size of the battery ( $7 \mu\text{m}$  effective pixel size, corresponding to  $15\text{--}20 \mu\text{m}$  physical resolution). Neutron tomography was carried out at the cold neutron radiography and tomography facility “CONRAD” at the reactor of the Hahn-Meitner-Institut Berlin. The facility is located at the end of a curved neutron guide and provides a very intense white beam with a flux of  $2 \times 10^8 \text{ n/cm}^2 \text{ s}$ . The used detector system consists of a 12 bit triggered CCD camera (Sensicam) with  $1280 \times 1024$  pixels and a LiZnS scintillator. The physical resolution was limited to about  $400 \mu\text{m}$  due to the energy dependent divergence caused by the neutron guide.

Two sizes of alkaline Zn– $\text{MnO}_2$  batteries were investigated: small AAAA (LR61) cells for synchrotron x-ray tomography and larger C (LR14) cells for neutron tomography. The batteries were discharged with a 10 or a  $2 \Omega$  resistor, respectively.

Figure 1 shows horizontal cross sections taken from the x-ray tomogram of an AAAA alkaline battery after 0, 90, and 180 min discharge time. The corresponding voltages after discharge were 1.59, 1.37, and 1.30 V. White corresponds to high x-ray attenuation coefficients and black to lower ones due to the common representation of tomographic data on a negative logarithmic scale. Beginning from the center of the battery, first the anode particles (white, A) in the electrolyte

gel (black) of the anode can be seen. They are surrounded by the separator (black, B) that consists only of weakly absorbing materials, mainly electrolyte. The  $\text{MnO}_2$  (gray, C) at the cathode builds a ring around the separator and is finally surrounded by the metal case (white).

The three images show exactly the same location in the battery. Figure 1(b) displays enlargements of the marked areas in Fig. 1(a). After a discharge time of 90 min some zinc particles were oxidized and partially dissolved and the local x-ray attenuation becomes weaker turning the gray scale in the images from white to bright gray: This demonstrates that ZnO can be easily separated from metallic Zn by tomography. The oxidation process begins in the outer regions of the anodic zone close to the separator and gradually moves towards the center of the battery, while increasingly more zinc particles are oxidized. After 180 min the ZnO forms a closed ring surrounding the remaining Zn particles. At this stage the voltage of the battery has dropped below the accepted value and can no longer be used. In contrast to previous studies this progressing oxidation effect can be observed *in situ* at the same location of the same battery.

To strengthen this *in situ* aspect of investigation, three-dimensional (3D) information is displayed in Fig. 1(c). It shows a further magnified bird’s-eye view of the zinc particles around the marked area in Fig. 1(b). ZnO and electrolyte are transparent, i.e., only metallic Zn is shown (threshold for the attenuation coefficient was  $9.2 \text{ cm}^{-1}$ ). The individual Zn particles and their spatial distribution can be seen very clearly. In the same area but after 90 min of discharge many of the smaller particles have disappeared because they are oxidized and are no longer included in the image due to their lower attenuation coefficient. The size of the larger particles is reduced as their outer part has been turned to oxide. As shown before, the process starts at the left side of the image that is assigned to the outer part of the zinc accumulation. After 180 min almost all smaller particles have been dissolved. Only at the right side small particles at the inner area are left. Even larger zinc particles with more than  $100 \mu\text{m}$  diameter have disappeared and only remnants of the two largest particles in the field of view are still visible.

By carrying out a 3D image analysis of the tomographic data the size distribution and the corresponding volume fractions of the metallic Zn particles were calculated [Fig. 1(d)].<sup>25,26</sup> The volume of each particle was used to calculate an effective particle diameter corresponding to a sphere of equal size. The diameters range between  $40$  and  $140 \mu\text{m}$  with a main peak at around  $72 \mu\text{m}$  which is also about the average diameter (calculated via the first moment of the distribution) of all Zn particles [dashed vertical lines in Fig. 1(d)]. Owing to the production process of the powder the particle size distribution can be approximated by a Gaussian curve.

After 90 and 180 min of electrical discharge a fraction of the zinc particles have been oxidized. Thus, the volume fraction of metallic zinc decreased [Fig. 1(d), center]. During oxidation the average size of the particles remains constant within the experimental error interval. This means that small and large particles are dissolved at almost the same rate due to the “layer-by-layer” oxidation of individual particles where at first the outer shell is almost completely oxidized before oxidation of deeper lying shells begins. Within a measurement volume of about  $1.2 \times 8.2 \times 8.2 \text{ mm}^3$  the amount of pure Zn and the Zn content in the ZnO were determined to

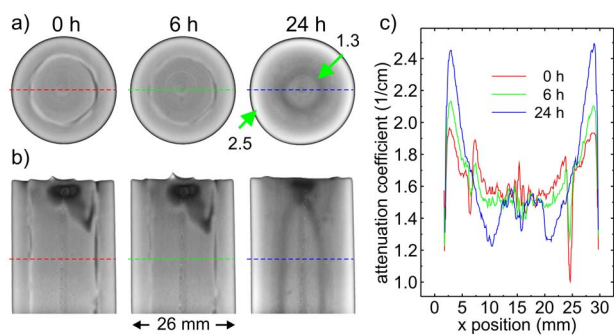


FIG. 2. (Color online) Images of a C-block-type alkaline battery in three different stages of discharge as obtained by neutron tomography. Horizontal (a) and vertical (b) cross sections of completely charged battery (left) and after two discharging steps (center and right), measured attenuation coefficients (in  $\text{cm}^{-1}$ ) are given in (a); (c) variation of the attenuation coefficient along the marked lines in (b).

be 58 and 1 mg in the (almost) fully charged state, 45 and 12 mg after 90 min, and 30 and 23 mg after 180 min, respectively. The values were calculated by taking the measured volumes of Zn and ZnO and the corresponding mean attenuation coefficients into account. Within the error intervals of about 7% the values prove that the overall amount of zinc remains almost constant during discharge. The slight decrease is attributed to the dissolution of the ZnO yielding attenuation coefficients which are excluded from the calculation by the threshold range (between 5.0 and 7.0  $\text{cm}^{-1}$ ).

Parallel to zinc oxidation on the anode side the  $\text{MnO}_2$  on the cathode side is swelling and breaking (some cracks are marked by red arrows in Fig. 1) with increasing discharge time [Fig. 1(a)]. The main reason for this is the hydrogen intercalation into the  $\text{MnO}_2$ . Neutron tomography allows us to quantify the distribution of intercalated hydrogen. Figure 2 shows cross sections through the tomogram of a C-block battery. Due to the resolution of 400  $\mu\text{m}$  metal, particles or cracks in the  $\text{MnO}_2$  are not visible here but the hydrogen density profile can be measured. In the fully charged battery [Fig. 2(b), left] no significant variations in the attenuation density both at the anode and the cathode are visible, but the images show variations in the electrolyte content inside the separator. The parts containing more electrolyte, possibly due to holes in the separator fleece, appear white while the regions with a very low amount of electrolyte are almost black.

After 6 and 24 h of discharge some hydrogen at the anode is lost and has moved to the cathode. Hydrogen is shifted from the outer regions of the anode where zinc is oxidized to the outer side of the cathode close to the steel case. This results in a white and a dark gray ring in the right image of Fig. 2(a) and white and dark gray stripes in the corresponding image of Fig. 2(b).

In Fig. 2(c) horizontal attenuation profiles through the axis of the battery in the three stages of discharge are compared. Again the decrease of the attenuation in the fully discharged battery (at  $x \approx 10$  mm and  $x \approx 20$  mm) is due to the loss of hydrogen that has moved to the outer sides of the battery (at  $x \approx 6$  mm and  $x \approx 30$  mm). The distribution of intercalated hydrogen within the cathode is not homogenous.

Most hydrogen can be found close to the steel case.

In conclusion, we have shown that synchrotron x-ray tomography and neutron tomography are excellent complementary methods for *in situ* investigation of alkaline batteries. The high spatial resolution of synchrotron tomography allows for analysis of the oxidation of individual zinc particles and the swelling and breaking of the  $\text{MnO}_2$  at the cathode. The size distributions of the zinc particles were calculated. We found that it is almost independent of the discharge time due to the layer-by-layer oxidation of the zinc gel. The hydrogen transport during discharge was visualized with neutron tomography. Hydrogen is intercalated into the  $\text{MnO}_2$  lattice predominantly at the edge close to the steel case. What has been demonstrated on commercial alkaline batteries could be also interesting for the investigation of rechargeable Zn– $\text{MnO}_2$  alkaline and other types of batteries in the future.

The authors would like to thank C. Reinhardt, G. Weidenmann, J. Goebbels, and B. R. Müller for their support with the experiments.

- <sup>1</sup>Q. C. Horn and Y. Shao-Horn, *J. Electrochem. Soc.* **150**, 652 (2003).
- <sup>2</sup>W.-B. Cai, Q. Shi, M. F. Mansuetto, and D. A. Scherson, *Electrochem. Solid-State Lett.* **3**, 319 (2000).
- <sup>3</sup>E. J. Podlaha and H. Y. Cheh, *J. Electrochem. Soc.* **141**, 15 (1994).
- <sup>4</sup>F. Cheng, J. Chen, X. Gou, and P. Shen, *Adv. Mater. (Weinheim, Ger.)* **17**, 2753 (2005).
- <sup>5</sup>L. Binder, K. Kordesch, and P. Urdl, *J. Electrochem. Soc.* **143**, 13 (1996).
- <sup>6</sup>A. Stani, W. Taucher-Mautner, K. Kordesch, and J. Daniel-Invad, *J. Power Sources* **153**, 405 (2006).
- <sup>7</sup>W.-B. Cai and D. A. Scherson, *J. Electrochem. Soc.* **150**, 217 (2003).
- <sup>8</sup>E. J. Podlaha and H. Y. Cheh, *J. Electrochem. Soc.* **141**, 28 (1994).
- <sup>9</sup>C. S. Johnson, D. W. Dees, M. F. Mansuetto, M. M. Thackeray, D. R. Vissers, D. Argyriou, C.-K. Loong, and L. Christensen, *J. Power Sources* **68**, 570 (1997).
- <sup>10</sup>Y. Mo, Y. Hu, I. T. Bae, O. B. Miller, M. R. Antonio, and D. A. Scherson, *J. Electrochem. Soc.* **144**, 1598 (1997).
- <sup>11</sup>Y. Paik, W. Bowden, T. Richards, R. Sirotna, and C. P. Greya, *J. Electrochem. Soc.* **151**, 998 (2004).
- <sup>12</sup>D. Im and A. Manthiram, *J. Electrochem. Soc.* **150**, 68 (2003).
- <sup>13</sup>S. Szpak and C. J. Gabriel, *J. Electrochem. Soc.* **126**, 1914 (1979).
- <sup>14</sup>*Handbook of Batteries*, edited by D. Linden and T. B. Reddy (McGraw-Hill, New York, 2002).
- <sup>15</sup>A. J. Bard, R. Parsons, and I. Jordan, *Standard Potentials in Aqueous Solution* (IUPAC, New York/Marcel Dekker, New York, 1985).
- <sup>16</sup>S. Turner and P. R. Buseck, *Nature (London)* **304**, 143 (1983).
- <sup>17</sup>R. W. Powers and M. W. Breiter, *J. Electrochem. Soc.* **116**, 719 (1969).
- <sup>18</sup>T. R. Thurston, N. M. Jisrawib, S. Mukerjee, X. Q. Yang, J. McBreen, M. L. Daroux, and X. K. Xing, *Appl. Phys. Lett.* **69**, 194 (1996).
- <sup>19</sup>D. Goers, M. Holzapfel, W. Scheifele, E. Lehmann, P. Vontobel, and P. Novák, *J. Power Sources* **130**, 221 (2004).
- <sup>20</sup>M. Lanz, E. Lehmann, R. Inhof, I. Exnar, and P. Novák, *J. Power Sources* **101**, 177 (2001).
- <sup>21</sup>L. Steinbock and C.-H. Dustmann, *J. Electrochem. Soc.* **148**, A132 (2001).
- <sup>22</sup>P. K. Sinha, P. Halleck, and C.-Y. Wang, *Electrochem. Solid-State Lett.* **9**, 344 (2006).
- <sup>23</sup>W. Graeff and K. Engelke, *Handbook on Synchrotron Radiation* (North-Holland, Amsterdam, 1991), Vol. 4.
- <sup>24</sup>W. Görner, M. P. Hentschel, B. R. Müller, H. Riesemeier, M. Krumrey, G. Ulm, W. Diete, U. Klein, and R. Frahm, *Nucl. Instrum. Methods Phys. Res. A* **467-468**, 703 (2001).
- <sup>25</sup>MAVI—Modular Algorithms for Volume Images, <http://www.itwm.fhg.de>
- <sup>26</sup>A. Rack, Ph.D. thesis, TU Berlin, 2006; <http://opus.kobv.de/tuberlin/volltexte/2006/1370/>